Journal of Oceanography, Vol. 56, pp. 643 to 654, 2000

Seasonal Variations of Water Masses and Sea Level in the Southwestern Part of the Okhotsk Sea

MOTOYO ITOH[1]* and KAY I. OHSHIMA[2]

[1]*Graduate School of Environmental Earth Science, Hokkaido University, Sapporo 060-0810, Japan*
[2]*Institute of Low Temperature Science, Hokkaido University, Sapporo 060-0819, Japan*

(Received 26 August 1999; in revised form 19 April 2000; accepted 13 June 2000)

A new grid data set for the southwestern part of the Okhotsk Sea was compiled by using all the available hydrographic data from the Japan Oceanographic Data Center, World Ocean Atlas 1994 and the other additional data sources with the resolution of about 10 km. We examine the seasonal variations of areas and volumes of Soya Warm Current Water (SWCW) and East Sakhalin Current Water (ESCW) and show that the exchanges of these water masses drastically occur in April and November. The peculiar variation of sea level in this region is also related with the water mass exchange. Sea level at the Hokkaido coast of the Okhotsk Sea reaches its minimum in April about two months later than in the case of ordinary mid-latitude ocean, and its maximum in December besides the summer peak. The winter peak of sea level in December is caused by the advent of fresh and cold ESCW which is accumulated at the subsurface layers (20–150 m) through the Ekman convergence by the prevailing northerly wind. Sea level minimum in April is caused by the release of the convergence and the recovery of dense SWCW that is saline and much colder than that in summer.

Keywords:
· Okhotsk Sea,
· Soya Warm Current Water,
· East Sakhalin Current Water,
· seasonal variation,
· water mass exchange,
· sea level,
· steric height,
· Ekman convergence.

1. Introduction

Southwestern part of the Okhotsk Sea is considered as a kind of confluence zone of two water masses. The one is warm and saline Soya Warm Current Water (referred to as SWCW hereinafter) which originates from the Sea of Japan and the other is cold and fresh East Sakhalin Current Water (referred to as ESCW) influenced by the discharge from the Amur River.

Warm saline water in the Sea of Japan enters into the Okhotsk Sea through the shallow Soya Strait (about 50 m) and flows along the coast of Hokkaido as the Soya Warm Current. Its water is the warmest and the most saline in the Okhotsk Sea. The driving force of the Soya Warm Current is ascribed originally to sea level difference between the Sea of Japan and the Okhotsk Sea (Aota, 1984; Ohshima, 1994). The Soya Warm Current shows strong seasonal variation in accordance with the sea level difference and the current variation is closely correlated with the sea level difference (Matsuyama *et al*., 1999). In summer the velocity of the Soya Warm Current reaches its maximum (Matsuyama *et al*., 1999) and the occupation width of its water becomes largest off Monbetsu (Aota, 1975). In winter it becomes very weak and intermittent and its water exists only near the bottom (Aota and Kawamura, 1978; Takizawa, 1982). Saline SWCW which is much colder than that in summer becomes as dense as $27.0\sigma_\theta$ in early spring (Takizawa, 1982). Watanabe and Wakatsuchi (1998) pointed out its importance in producing the origin water of North Pacific Intermediate Water (NPIW).

The East Sakhalin Current flows along the eastern coast of Sakhalin and brings low salinity water originating from the Amur River. Watanabe (1963) suggested, on the basis of the salinity distribution and the sea ice drift, that the East Sakhalin Current leaves the coast off Cape Terpenia and turns to the east toward the Kuril Basin in summer. It flows southward along the coast and reaches the Hokkaido coast in autumn and winter. Surface salinity off the Hokkaido coast drops suddenly being less than 32.0 in November or December, which is an indication of the influence of ESCW (Watanabe, 1963; Akagawa, 1977).

Other feature in this region is that sea ice is brought by both the East Sakhalin Current and the northerly wind in winter, which makes this region ice-covered sea in spite of low latitude. It is also noted that sea level at the

* Corresponding author. E-mail: motoyo@lowtem.hokudai.ac.jp

Hokkaido coast of the Okhotsk Sea tends to show the secondary maximum in winter besides the summer peak (Konishi *et al*., 1986), probably reflecting the water mass exchange.

All the previous oceanographic studies for this region were based on snapshot observations, which include interannual, seasonal and shorter-period variabilities. Although oceanographic observations in whole the Okhotsk Sea are still limited, only for the southwestern part of the Okhotsk Sea dense routine observation network has been executed by several Japanese Agencies for many years. Thus the sufficient data have been accumulated for describing the climatology of temperature and salinity field with a relatively high resolution.

In order to extract pure seasonal variation, monthly, seasonal and annual grid data set for temperature and salinity with the resolution of about 10 km were compiled for this study, by using all the available historical data. Since limited description has been made for ESCW in the southwestern area of the Okhotsk Sea up to date, this study provides more detailed description of its spatial and seasonal variations. An advantage of grid data set is that the volume of each water mass can be calculated. Thus we focus on the water mass exchange of SWCW and ESCW based on the calculation of their volume change. Further we consider the responsible factor for the peculiar variation of sea level in this region by comparison with the variations of steric height and water mass. Finally we intent to propose a possible driving mechanism for the water mass exchange.

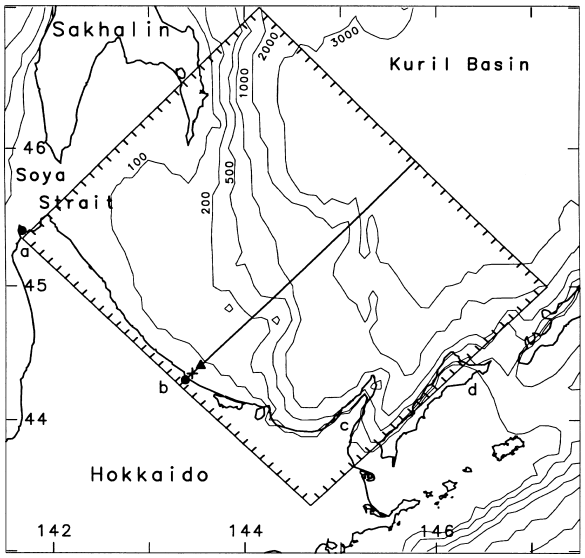

Fig. 1. Bathymetry of the southwestern part of the Okhotsk Sea and the grids for which data set is made. Triangle indicates the grid at which T-S diagrams are shown in Fig. 7. Cross indicates the grid at which geopotential thickness anomaly is shown in Fig. 13. At the Triangle and cross points steric height is also calculated in Fig. 12. The line off Monbetsu is the section on which vertical distribution of salinity is shown in Fig. 6. The labeled dots denote the followings; a: Wakkanai, b: Monbetsu, c: Shiretoko Peninsula, and d: Kunashiri Island.

2. Data and Method

We make new temperature and salinity grid data set for the southwestern part of the Okhotsk Sea. Study area is enclosed by solid line in Fig. 1. The grid spacing is taken about 10 km. In this region there is a strong frontal feature along the Hokkaido coast between inshore saline SWCW and offshore less saline water. The coordinate system is taken parallel with the coast as shown in Fig. 1 to better resolute SWCW and its frontal feature. Because the data is very limited in the northern part, grid data set is made only for south of 46°N.

The historical hydrographic data used in this study are obtained mainly from the Japan Oceanographic Data Center (JODC) and World Ocean Atlas 1994 (WOA94). Data collection in February and March is extremely limited because of severe winter and ice coverage. Thus we add the observational data taken by the icebreaker "Soya" in February from 1996 to 1998 under the cooperation of Hokkaido University and the Japan Coast Guard. This addition to the data-void season enables us to discuss the full annual cycle. We also add the observational data taken by the Hokkaido Fisheries Agency and the Japan Coast Guard, which have not yet been incorporated into the JODC and WOA94 digital archives. The oceanographic data consists of Nansen casts and conductivity/salinity-temperature-depth (C/STD) casts. We only use the data which have both temperature and salinity components. Data set is made for 20 standard depth levels (0, 10, 20, 30, 50, 75, 100, 125, 150, 200, 250, 300, 400, 500, 600, 700, 800, 1000, 1200 and 1500 m).

Generally, shallower the depth, larger the seasonal variation and data amounts. Hence, monthly mean data set is made for the depths from 0 to 150 m, seasonal mean data set is made for the depths from 200 to 400 m and for the depths from 500 to 1500 m only annual mean data set is made. In this study, we define winter as December–February, spring as March–May, summer as June–August and autumn as September–November.

Prior to objective analysis, statistical check is performed to eliminate outliers as follows. All the data for temperature and salinity at each standard level is averaged by one grid box to produce a record number of observations, mean value and standard deviation in each grid box. A two standard deviation criterion is applied to eliminate individual observation for further use in our objective analysis. Figure 2 shows the spatial distribution of all the quality-controlled data points.

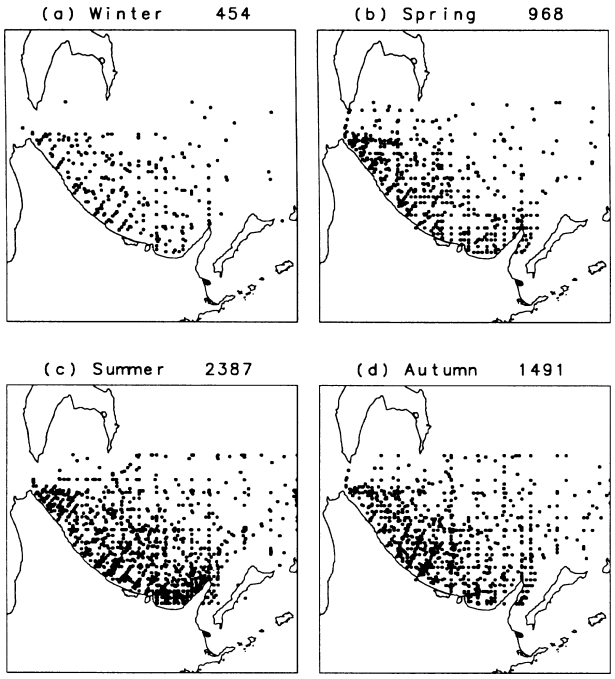

Fig. 2. Spatial distributions of hydrographic stations used in this study. (a) winter (December–February), (b) spring (March–May), (c) summer (June–August) and (d) autumn (September–November). Numbers in the upper right-hand corner are the record numbers of observations.

We applied similar objective analysis method used by Barens (1964) and Levitus (1982). We calculate the autocorrelation functions of temperature and salinity from 0–150 m layers where the sufficient data exist. The autocorrelation function is quite different between inshore and offshore regions because of the existence of SWCW and its sharp front near the coast. It can be the best fit in the Gaussian distribution with the e-folding scale being ~25 km for the inshore region and ~45 km for the offshore region. For making grid data set from the station data, we use the Gaussian distribution as the weight function with the e-folding scale increasing linearly from 25 km to 45 km from the coast to the offshore, and we set the weight function zero when the distance between observational point and the grid point is more than twice of the e-folding scale. We call this zero criterion as influence radius. If the data number within the influence radius is less than 10, the influence radius is increased by 25 km. When the influence radius becomes more than 125 km, that grid box is regarded as no data. This criterion is relaxed only for calculation of the volumes of SWCW and ESCW in Section 4. The influence radius is increased further until the data number within the influence radius reach the minimum requirement of 10. This does not effect the result much since the grid boxes with no data exist in the northeastern part of the study area where SWCW and ESCW do not exist usually. Since in March the data collection is extremely limited and the area of no data is large, March is excluded in our analysis.

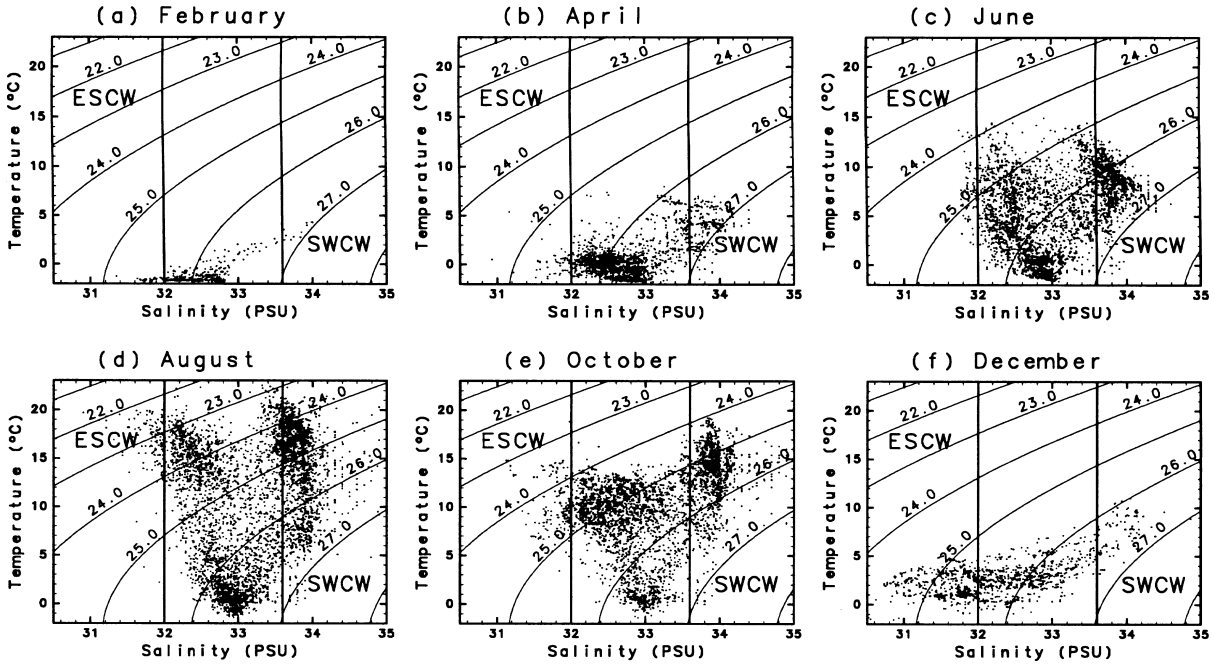

Fig. 3. Bimonthly variations in Temperature (°C)-Salinity diagrams from all the raw data from 0 to 50 m depths. Contours denote isolines of the potential density and contour intervals are $1.0\sigma_\theta$.

3. Seasonal Variations of Water Properties

We here describe seasonal variation of oceanographic condition from grid data set. In the southwestern part of the Okhotsk Sea, there are two identifiable groups of water masses, SWCW and ESCW. First we will give definition of these two water masses. Figure 3 shows Temperature-Salinity (T-S) diagrams for every two month from all the raw data in the depths of 0–50 m. As it will be described in Section 4, SWCW is dominant in the depths of 20–50 m and ESCW is dominant in the surface layer. Thus we show T-S diagrams for the depths shallower than 50 m to demonstrate the seasonal variations of SWCW and ESCW. The water in the surface layer in the Okhotsk Sea except SWCW and ESCW has the salinity ranging around 32.0–

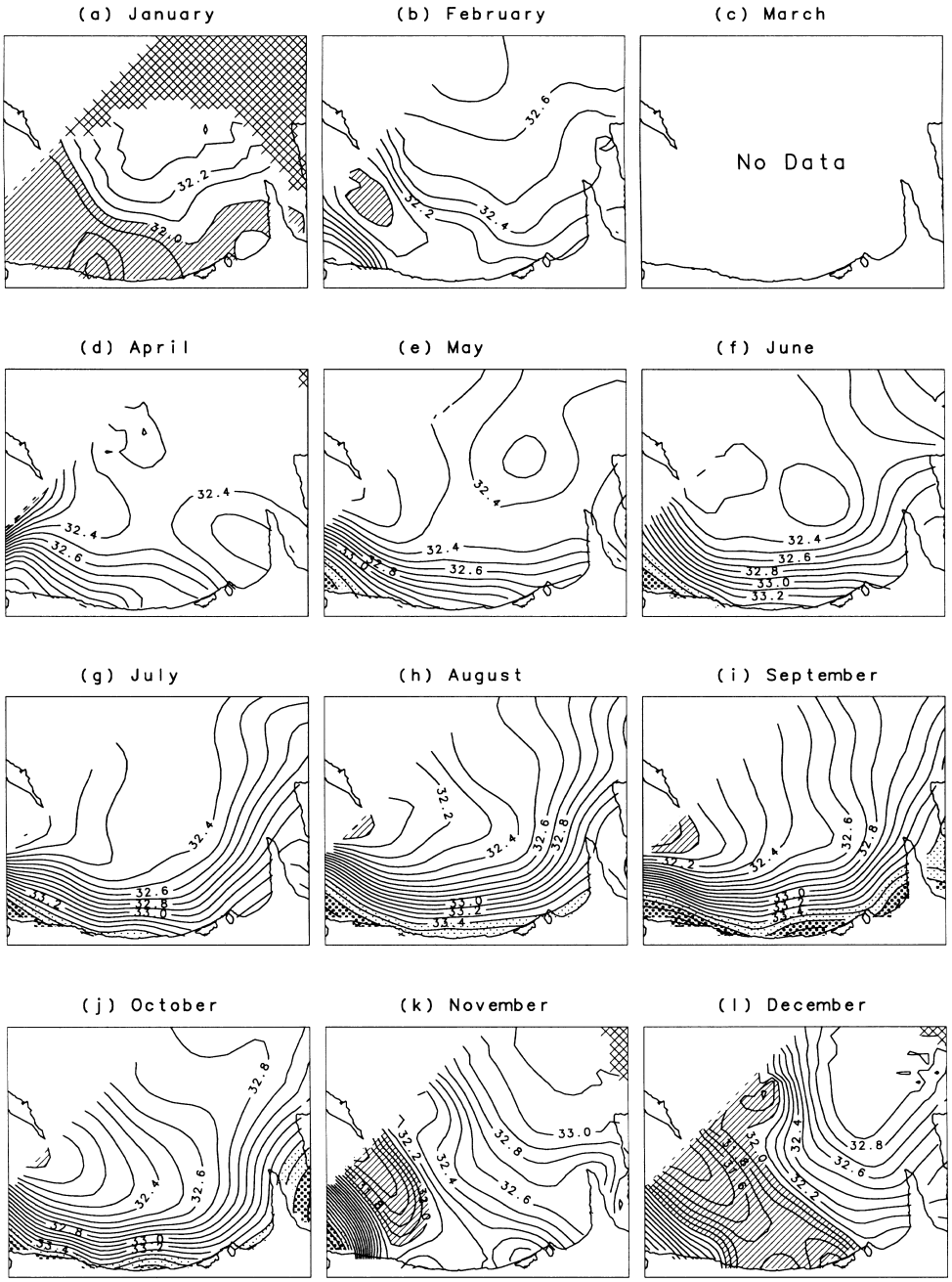

Fig. 4. Monthly variations of the horizontal salinity distributions at sea surface. Contour intervals are 0.1. The area of SWCW (more than 33.6) is dotted and the area of ESCW (less than 32.0) is shaded, respectively. The area with salinity more than 33.4 is lightly dotted. The area where the influence radius becomes more than 125 km is cross shaded.

33.6 throughout the year. A group having salinity of 33.6–34.2 from April to October in Fig. 3 corresponds to SWCW and low salinity water of 31.0–32.0 which is dominant in December corresponds to ESCW. In this paper, we define SWCW as the water with salinity higher than 33.6 and ESCW less than 32.0 on the basis of Fig. 3, Aota (1975) and Takizawa (1982). Takizawa (1982) gave more precise definition for water masses. He divided SWCW into two water masses according to the temperature ranges: SWCW and the Forerunner of Soya Warm Current Water (referred to as FSWCW). The water that comes from the Sea of Japan in early spring (April–May) is particularly cold and Takizawa (1982) called this water as FSWCW. As shown in Fig. 3 temperature of SWCW changes considerably depending on season, while salinity of SWCW does not change much and remains higher

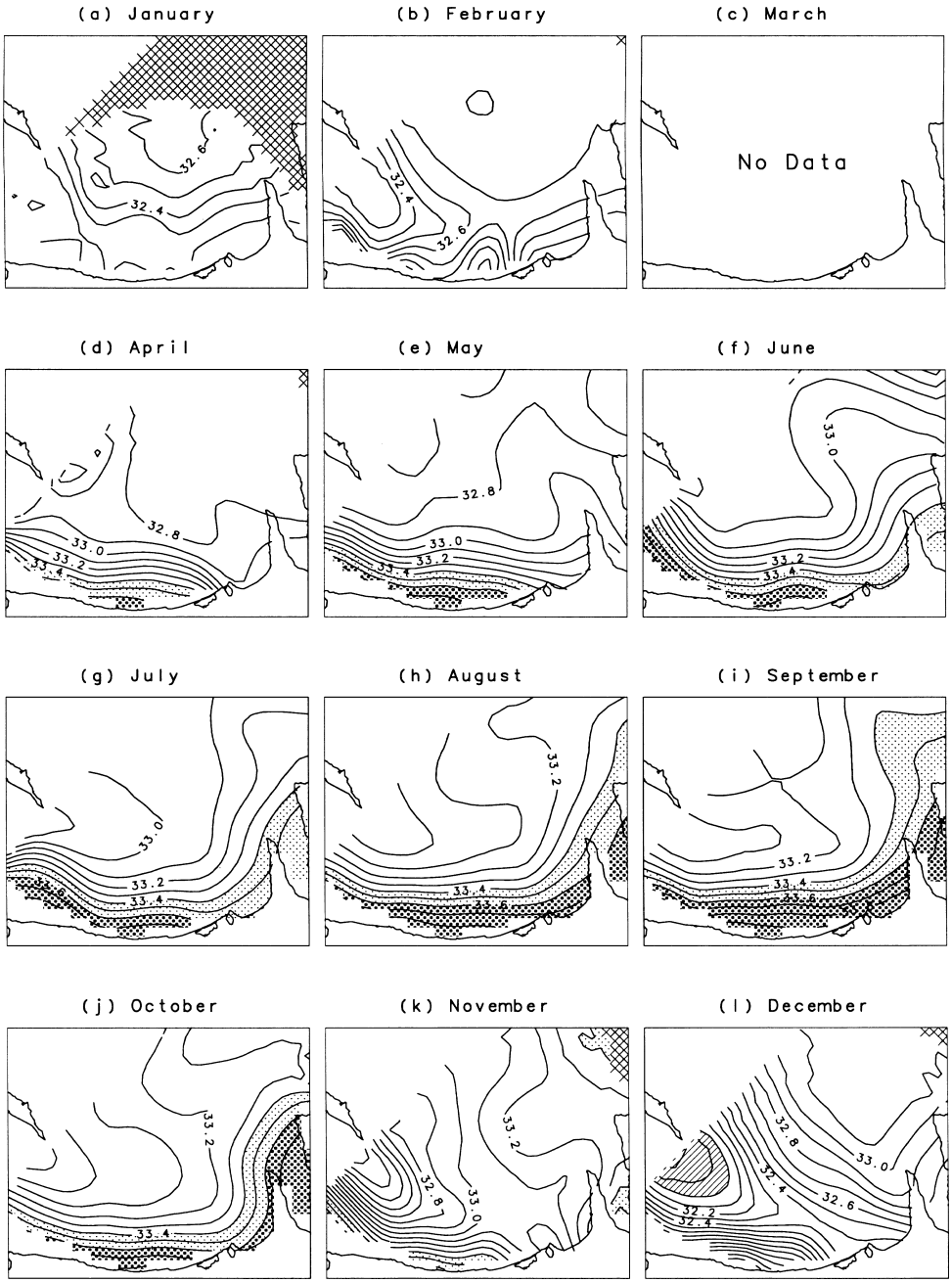

Fig. 5. Monthly variations of the horizontal salinity distributions at 50 m depth. Intervals of contour lines are 0.1. The shading and dotting are done in the same way as in Fig. 4.

than 33.6 throughout the year. Thus the identification of water mass is made only by salinity and we refer to both SWCW and FSWCW as SWCW in this paper.

Figures 4 and 5 show the monthly salinity distributions at the depths of 0 and 50 m, respectively. Figure 6 shows the monthly vertical sections of salinity off Monbetsu. The area of SWCW is dotted and the area of ESCW is shaded in Figs. 4, 5 and 6, respectively. The area with salinity more than 33.4 is also lightly dotted to show diluted SWCW.

Regarding to the seasonal variation of ESCW, ESCW appears in the vicinity of the southern tip of Sakhalin from August and remains there until October in the surface layer as shown in Fig. 4. This fresh ESCW starts to spread southward along the shelf break in November and reaches to the Hokkaido coast off Monbetsu in December. South-

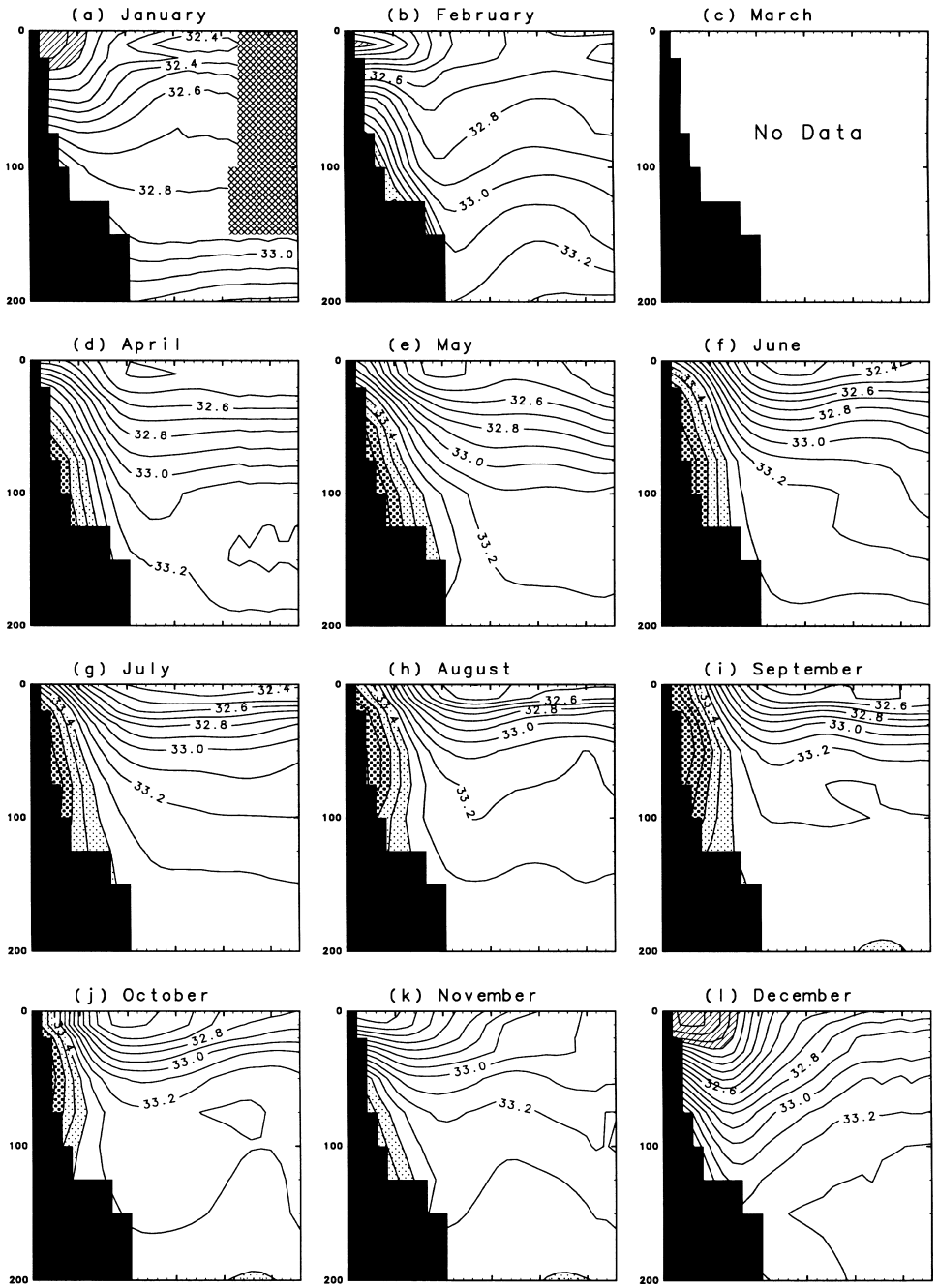

Fig. 6. Monthly variations of vertical salinity section off Monbetsu shown in Fig. 1. Contour intervals are 0.1. The shading and dotting are done in the same way as in Fig. 4.

ward extension of less saline water can be also seen at the depth of 50 m (Fig. 5). It is found from the vertical sections of salinity in December and February (Fig. 6) that the surface layer with less saline water shows the downwelling feature at the shelf slope. Although this feature is not clear in January, it is probably due to the limited data available in the offshore region. In January ESCW spreads towards the Soya Strait and the Shiretoko Peninsula in the surface layer (Fig. 4). Its salinity gradually increases in February and ESCW nearly disappears by April. The downwelling feature also disappears by April. Watanabe (1995) showed that in winter the averaged density from 0 to 250 m decreases near the Hokkaido coast and suggested that coastal downwelling by the northerly wind is a possible mechanism for this feature.

Regarding to the seasonal variation of SWCW, SWCW in the surface layer (Fig. 4) exists only near the Soya Strait from May to June, while it gradually extends southeastward along the Hokkaido coast from July to October. High salinity water can be traced to Kunashiri Island along the depth contour of 100 m. The area of SWCW in the surface rapidly shrinks and exists only near the Soya Strait in November and finally disappears from December to April. As shown in Fig. 5, SWCW is dominant in the layer of 50 m. SWCW reaches near Monbetsu at the depth of 50 m in April although it is not recognized in the surface. It expands its width and extends further downstream in summer. In September the area of SWCW becomes its maximum and reaches near Kunashiri Island. SWCW disappears in December and does not exist until February. Vertical sections of salinity (Fig. 6) demonstrate

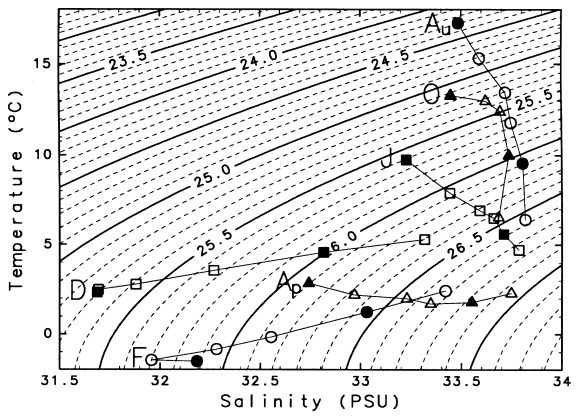

Fig. 7. Bimonthly variation in Temperature (°C)-Salinity diagram at the grid point off Monbetsu from 0 to 75 m depths. Location of the grid point is shown by the triangle in Fig. 1. Contours denote isolines of the potential density and contour intervals are $0.1\sigma_\theta$. February and August are designated by circles, June and December by squares, April and October by triangles. Solid characters indicate the data at the depths of 0 and 50 m.

that SWCW appears only near the bottom in early spring from April to May.

Figure 7 shows the seasonal variation in Temperature-Salinity diagram of the grid data for every two month near Monbetsu from 0 to 75 m. This figure clearly demonstrates exchange of water masses: warm and saline SWCW from spring to summer is replaced by cold and fresh ESCW from autumn to winter. As Watanabe (1963) point out that ESCW exists only above 50 m, it is also shown from grid data set that fresh ESCW less than 32.0 is confined to the shallower depths (Figs. 6(a) and (l)). However, significant decrease of salinity also occurs at deeper water at 75 m (Fig. 7) and from 75 to 150 m (Fig. 6(l)). It is found from Fig. 7 that SWCW becomes the densest in April, reaching as dense as $26.9\sigma_\theta$. Watanabe and Wakatsuchi (1998) suggested from a snap shot observation that SWCW in early spring reaches as dense as the density of NPIW ($26.8–26.9\sigma_\theta$) and that it is a possible source of origin water of NPIW. The climatological data set also indicate that SWCW becomes as dense as $26.9\sigma_\theta$ in early spring.

4. Volumetric Analysis of Soya Warm Current Water and East Sakhalin Current Water

With the definition of SWCW as having salinity higher than 33.6 and ESCW as having salinity less than 32.0, we calculate the seasonal variations of areas at several depths (Fig. 8) and volumes (Fig. 9) of them, respectively.

We calculate the seasonal variations in their occupying areas at the depths of 0, 20, 50 and 100 m, respectively (Fig. 8). It is found that SWCW is dominant in the depths of 20 and 50 m. The area of SWCW increases from spring to summer and its maximum occurs in September for all depths. SWCW decreases drastically in November. These features are consistent with the observations off Monbetsu by Aota (1975). Aota (1975) and Takizawa (1982) showed that SWCW still exists in winter, although it is very weak and intermittent. In our data set, however, SWCW is not recognized from December to February for all depths. One reason for this is a result of the mixing of small volume of SWCW with surrounding low salinity water. The other is that the averaging procedure hides the intermittent phenomena. In fact some of the raw data in Fig. 3(a) show the properties of SWCW having salinity higher than 33.6 in winter. Area of ESCW increases rapidly from November to December. It becomes its maximum in December or January and then decreases in February. ESCW is confined to the shallower depths and does not exist for the depths greater than 50 m.

Figure 9 shows the seasonal variations of the volumes of SWCW and ESCW from 0 to 150 m depths. These values represent the total volumes of SWCW and ESCW in the study area, since both SWCW and ESCW exist only

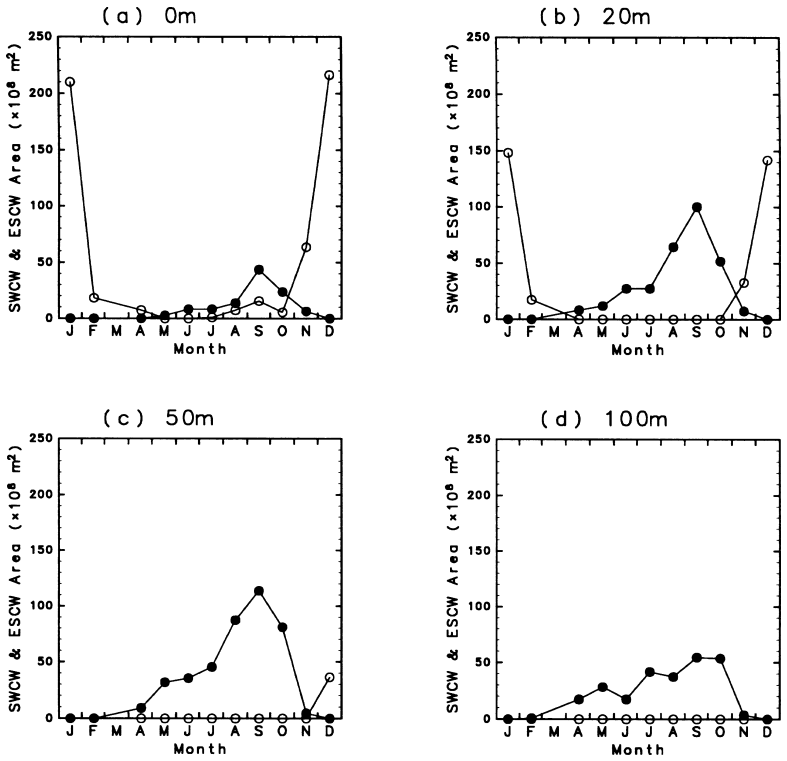

Fig. 8. Seasonal variations in the occupied area of Soya Warm Current Water (solid circles; water with salinity more than 33.6) and East Sakhalin Current Water (open circles; water with salinity less than 32.0) at (a) 0 m, (b) 20 m, (c) 50 m and (d) 100 m in the study area. Unit is 10^8 square meters.

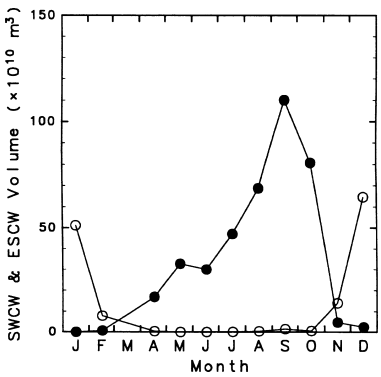

Fig. 9. Seasonal variations in the volume of Soya Warm Current Water (solid circles; water with salinity more than 33.6) and East Sakhalin Current Water (open circles; water with salinity less than 32.0) from 0 to 150 m depths in the study area. Unit is 10^{10} cubic meters.

above 150 m according to our definition. This figure clearly demonstrates the exchange of two water masses. SWCW increases in summer with its maximum in September, and then rapidly decreases in November. At the same time, ESCW increases rapidly in November with its maximum in December and then it rapidly decreases in February. In April, ESCW nearly disappears while SWCW recovers instead. Drastic exchanges of water masses occur in April and in November.

5. Seasonal Variations of Sea Level and Water Mass Exchange

Watanabe (1963) and Akagawa (1977) showed that density and salinity in the sea surface drop off Monbetsu suddenly in November or December according to the advent of fresh ESCW. Konishi *et al.* (1986) showed that sea level at the Hokkaido coast of the Okhotsk Sea tends to show the secondary maximum in winter besides the summer peak. Density decrease due to ESCW is probably related to sea level rise at the coast, and correspondingly the peculiar variation of sea level is probably related to the water mass exchange. Here we compare the seasonal variation of sea level observed by the tide gauges with that from steric height of grid data set and then examine the responsible factor for the peculiar variation of sea level.

The seasonal variation of sea level at Wakkanai and Monbetsu is shown in Figs. 10(a) and (b), respectively. Sea level is barometrically adjusted by atmospheric pressure, with 1 cm corresponding to 1 hPa. Sea level and

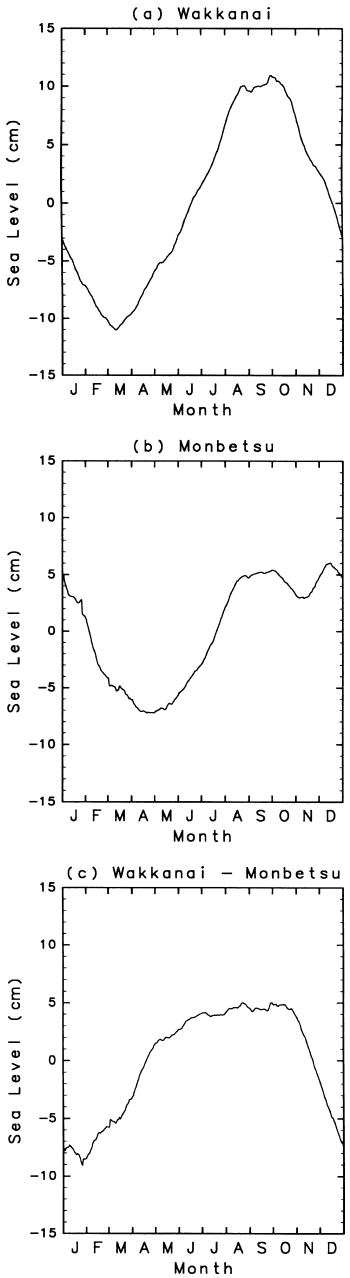

Fig. 10. Seasonal variations of sea level (cm) at (a) Wakkanai, (b) Monbetsu, and (c) their difference (Wakkanai–Monbetsu).

atmospheric pressure data are provided by JODC and Japan Meteorological Agency, respectively. Mean sea level for 20 years from 1965 to 1985 is calculated with 31 days running mean, on the basis of the hourly data. Generally in the mid-latitude of the northern hemisphere, sea level becomes its maximum in August or September and minimum in February or March, e.g., Wakkanai (Fig. 10(a)), accordingly to the atmospheric heating-cooling cycle. Sea level variation at Monbetsu does not show such simple

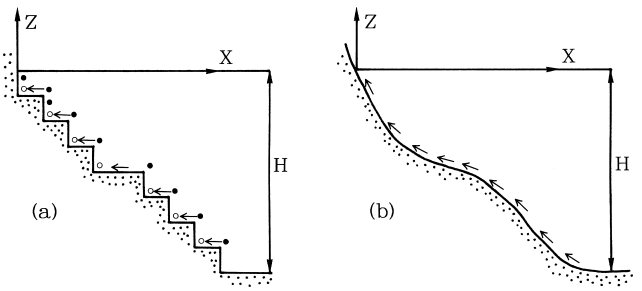

Fig. 11. Schematic figures of integration path of steric height. (a) Extrapolation method used in our calculation. The value of geopotential anomaly at the bottom layer (open circle) is extrapolated by extending that of the next offshore grid point horizontally as shown by arrow. (b) Integration path in the theory of Csanady (1979).

seasonal cycle, correspondingly it becomes its maximum in December besides the summer peak and reaches its minimum in April, one or two months later than the ordinary case. This feature seems to be common to the Hokkaido coast of the Okhotsk Sea, since sea level at Abashiri also shows the similar variation to that of Monbetsu.

Next we compare the seasonal variation of sea level from the tide gauge with that from steric height near the tide gauge station of grid data set. For calculation of steric height at the point shallower than the reference depth, the value of geopotential anomaly at the bottom layer (open circle in Fig. 11(a)) is extrapolated by extending that of the next offshore grid point (solid circle) horizontally, as schematically shown in Fig. 11(a). Similar extrapolation was adopted by several studies and the validity of this extrapolation was demonstrated in them. Sturges (1974) applied this extrapolation method to alongshore the Pacific coast of the United States of America, and Reid and Mantyla (1976) to the northern North Pacific. Both of them showed that the seasonal variations of steric height and the inshore tide gauge are in good agreement. Since this extrapolation method was somewhat a temporary expedient, Csanady (1979) gave a theoretical justification to this method on the basis of the equations of motion. He examined how the surface pressure field (and accordingly sea level) made by the spatial distributions of the density (or dynamic depth) run into the shallower coastal region. He assumed the alongshore uniformity of physical properties. When no wind stress is applied and sea level elevation at the deep ocean is constant in the alongshore direction, the bottom Reynolds stress must be zero everywhere. If the bottom stress is caused by the bottom velocity, the bottom velocity should vanish. In this case steric height at the coast Φ ($x = 0$) is reduced to the following equation.

$$\Phi\ (x=0) = \int_{-H}^{0} \rho_0 g \delta_b dz.$$

δ_b is specific volume anomaly at the bottom. Specific volume anomaly δ is defined as $\alpha(S, T, p) - \alpha(35, 0, p)$. $\alpha(S, T, p)$ is specific volume of sample water at salinity S, temperature T, and pressure p. $\alpha(35, 0, p)$ is standard water of $S = 35$, $T = 0$ and pressure p. The quantity ρ_0 represents a constant density magnitude 1.02 in units of per cubic centimeter. Csanady (1979) used the density deficit from the reference density instead of specific volume anomaly. Although our expression is somewhat different from that of Csanady (1979), the content is basically the same. Figure 11(b) is the schematic figure of the integrated path in the calculation of this theory. The path is along the sea floor from the reference depth H toward the coast. Under the relatively fine grid resolution, our extrapolation method can be nearly consistent with this theory.

Here we calculate sea level at the triangle and cross points from steric height relative to 1500 m setting the line off Monbetsu (see Fig. 1). Around this line the alongshore uniformity is satisfied as the first approximation. It should be noted that sea level variation is not explained only from the steric height variation. The barotropic current, which extends to the bottom, may also affect sea level. Actually the Soya Warm Current has barotropic feature (Aota, 1984). In this study we are unable to examine effect of barotropic component.

Comparing Fig. 12 with Fig. 10(b), the seasonal variation of the sea level from steric height is very similar to that from the tide gauge. The summer and winter maximums and spring minimum of steric height coincide with those of sea level. Responsible factors for this particular sea level variation are examined by using grid temperature and salinity data set. We should strictly use data at the most inshore grid point (cross point in Fig. 1). Since the two lines in Fig. 12 are very similar, we adopt the data at the triangle point.

Figure 13 shows the seasonal variation of geopotential thickness anomaly between the two constant depth surfaces at triangle point. Each line denotes the anomaly from the annual mean of geopotential thickness between the two layers. We show the result only for the layers less than 150 m, since at the deeper layers the seasonal variation of geopotential thickness is very small. We divide these into four layers; 0–20 m, 20–50 m, 50–100 m and 100–150 m. Figure 13 demonstrates which layer contributes to each peak of steric height (and accordingly sea level). Figure 13 shows that 0–50 m layers mainly contribute to the summer peak in August and 20–150 m layers mainly contribute to the winter peak in December. On the other hand, all layers contribute to sea level minimum in April.

Then we examine which component of temperature or salinity contributes to each peak of sea level, using T-S diagram of Fig. 7 and salinity vertical sections of Fig. 6. We first focus on the difference of the two peaks: summer peak and winter peak. Salinity decreases at all depths from August to December according to the increase of surface fresh ESCW (Fig. 7) and the accumulation of less saline water at the subsurface layers through downwelling (Fig. 6 (l)). In this period temperature in the layers from 0 to 20 m decreases drastically and thus the density in that layers increases because of the dominance of temperature effect on the density as shown in Fig. 7. In con-

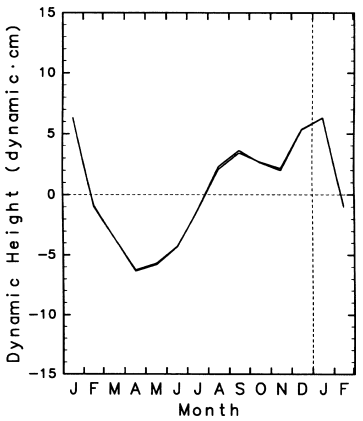

Fig. 12. Seasonal variations of steric height (dynamic centimeter) at the two grid points off Monbetsu relative to 1500 m. The location of the gird points are shown by cross and triangle in Fig. 1.

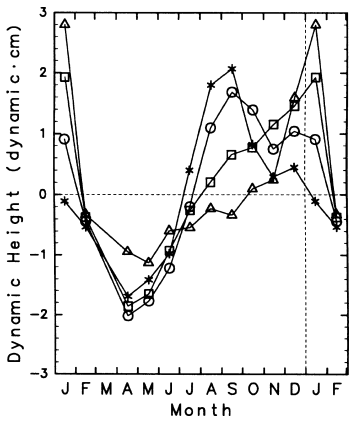

Fig. 13. Monthly variations of geopotential thickness anomaly (dynamic centimeter) between two constant depths off Monbetsu. Each line denotes anomaly from annual mean of geopotential thickness. Asterisks indicate layer from 0 to 20 m, circles that from 20 to 50 m, squares that from 50 to 100 m, triangles that from 100 to 150 m. Location of the gird point is shown by cross in Fig. 1.

trast, at subsurface layers deeper than 30 m the density decreases because of the dominance of salinity effect on the density. Thus the winter peak in December of sea level arises from salinity drop at subsurface layers not from the surface layers. On the other hand, the summer peak in August arises from the surface heating.

Next sea level minimum in April is considered. Temperature reaches its minimum in February and it is colder than that in April for all depths as shown in Fig. 7. Because of more saline water of the Soya Warm Current, the density in April becomes larger than that in February for all depths. In June the density becomes smaller than that in April because of warming of SWCW. The release of the downwelling feature also occurs in spring as shown in Fig. 6(d). In brief, the delay of sea level minimum is ascribed to the release of the downwelling and the recovery of dense SWCW.

6. Summary and Discussion

By using all the available hydrographic data, we have made new grid data set with the high resolution for the southwestern part of the Okhotsk Sea. On the basis of this data set, we have shown the seasonal variations of Soya Warm Current Water (SWCW) and East Sakhalin Current Water (ESCW), and clarified the responsible factor for the peculiar sea level variation in this region.

From climatological data set, the areas of SWCW are most developed in the depths of 20 and 50 m (Fig. 8). In April SWCW begins to recover from the bottom and becomes densest, reaching as dense as $26.9\sigma_\theta$, the density of North Pacific Intermediate Water (NPIW) in Fig. 7. From spring to summer SWCW expands its width and extends further downstream, with its maximum in September (Figs. 4 and 5). During summer season ESCW exists only in the vicinity of southern tip of the Sakhalin (Fig. 4). The area of SWCW rapidly decreases in November, while the area of ESCW increases instead and it spreads southward along the shelf break. In December ESCW reaches the Hokkaido coast (Fig. 4) and it is accumulated and downwelled at the subsurface layers (Fig. 6). During winter its salinity gradually increases probably due to brine rejection by sea ice formation and/or vertical mixing in situ or upstream. ESCW nearly disappears and downwelling feature is released by April (Figs. 4 and 6). It can be shown, from the seasonal variations of the areas and volumes of SWCW and ESCW, that drastic water mass exchanges occur in April and in November in this region (Figs. 8 and 9).

The peculiar seasonal variation of sea level in this region is closely related with this water mass exchange. Sea level at the Hokkaido coast of the Okhotsk Sea becomes its minimum in April, one or two months later than the timing of sea surface temperature minimum, and becomes its maximum in December besides the summer peak in August (Fig. 10(b)). The seasonal variation of sea level at Monbetsu observed by the tide gauge is very similar to that from steric height near the coast from our data set (Fig. 12). Then we examined the responsible factor for the variation from temperature and salinity data (Figs. 13, 6 and 7). The winter peak of sea level is caused by the advent of fresh and cold ESCW that is accumulated at the subsurface layers (20–150 m). This accumulation feature is probably due to the Ekman convergence by the prevailing northerly wind. In April the release of the Ekman convergence and the recovery of cold and saline SWCW cause sea level minimum. The winter peak of sea level depends on the timing of the ESCW advent. The oceanographic data in autumn and winter is too scarce to discuss the interannual variability of the East Sakhalin Current. However, by using sea level data accumulated for more than 30 years, discussion of the interannual variability of the ESCW advent will become possible.

Finally we briefly discuss the driving mechanism of the water mass exchange in this region. Sea level in the Sea of Japan is generally higher than that in the Okhotsk Sea. Thus warm saline SWCW steadily enters the Okhotsk Sea from the Sea of Japan. However, its strength shows distinct seasonal variation in accordance with the seasonal variation of the sea level difference. At the Hokkaido coast of the Okhotsk Sea, sea level elevation can be affected not only by the heating and cooling cycle but also by the advent of ESCW and the Ekman convergence in winter. Because of the dominance of the northerly and northwesterly wind from October, the East Sakhalin Current is strengthened and ESCW influenced by the discharge from the Amur River is transported southward. ESCW reaches the Hokkaido coast in late November. The advent of ESCW with accumulation of less dense water due to the Ekman convergence leads to sea level rise at the Hokkaido coast, consequently reducing sea level difference between the Sea of Japan and the Okhotsk Sea. Thus the Soya Warm Current driven by the sea level difference is weaken in winter. At the shallow Soya Strait, this sea level rise seems to be felt barotropically, since it is mainly caused by salinity decrease at the deeper layers than the bottom depth of the strait. In the spring season (March–April), the northerly wind becomes weak and the Ekman convergence is released. This leads to sea level drop in the Okhotsk Sea and correspondingly the sea level difference recovers slightly (Fig. 10(c)), which might trigger the reinforcement of the Soya Warm Current.

Acknowledgements

We acknowledge Shoshiro Minobe and Tatsuro Watanabe for data processing. We are grateful to Masaaki Wakatsuchi, Motoyoshi Ikeda, Yasushi Fukamachi, and Genta Mizuta for their useful discussion. We are greatly appreciate the captains and crew members of icebreaker

"Soya" of the Hydrographic Department of Japan Coast Guard for their supports in the observations. Comments by three anonymous reviewers improved the text. Figures were produced by GFD DENNOU Library. This work was supported by the International Cooperative Research Program on Global Ocean Observing System (1993–1997).

References

Akagawa, M. (1977): Characteristics of oceanographic conditions in the Okhotsk Sea and meteorological conditions over the Far East in November. *Oceanogr. Mag.*, **28**, 33–45.

Aota, M. (1975): Studies on the Soya Warm Current. *Teion Kagaku*, **33**, 151–172 (in Japanese).

Aota, M. (1984): Oceanographic structure of the Soya Warm Current. *Bull. Coast Oceanogr.*, **22**, 30–39 (in Japanese).

Aota, M. and T. Kawamura (1978): Observation of oceanographic condition in the Okhotsk Sea coast of Hokkaido in winter. *Teion Kagaku*, **37**, 93–105 (in Japanese).

Barnes, L. S. (1964): A technique for maximizing details in numerical weather map atlas. *J. Appl. Meteorol.*, **3**, 396–409.

Csanady, G. T. (1979): The pressure field along the western margin of the North Atlantic. *J. Geophys. Res.*, **81**(C8), 4905–4915.

Konishi, T., E. Kamie and T. Segawa (1986): Characteristics of tides along the coast of Japan. *Kaiyo Kagaku*, **18**(7), 437–441 (in Japanese).

Levitus, S. (1982): Climatological Atlas of the World Ocean. NOAA Prof. Pap., 13, 173 pp.

Matsuyama, M., M. Aota, I. Ogasawara and S. Matsuyama (1999): Seasonal variation of Soya Current. *Umi no Kenkyu*, **8**, 333–338 (in Japanese with English abstract).

Ohshima, K. I. (1994): The flow system in the Sea of Japan caused by a sea level difference through shallow straits. *J. Geophys. Res.*, **99**(C5), 9925–9940.

Reid, J. L. and A. W. Mantyla (1976): The effect of the geostrophic flow upon coastal sea elevations in the northern North Pacific Ocean. *J. Geophys. Res.*, **81**(18), 3100–3110.

Sturges, W. (1974): Sea level slope along continental boundary. *J. Geophys. Res.*, **79**(6), 825–830.

Takizawa, T. (1982): Characteristics of the Soya Warm Current in the Okhotsk Sea. *J. Oceanogr. Soc. Japan*, **38**, 281–292.

Watanabe, K. (1963): On the reinforcement of the East Sakhalin Current preceding to the sea ice season off the coast of Hokkaido. *Oceanogr. Mag.*, **14**, 117–130.

Watanabe, T. (1995): Water characteristics in the Kuril Basin of the Sea of Okhotsk, with emphasis on low density water. Ph.D. Dissertation, Hokkaido University, Sapporo, 69 pp.

Watanabe, T. and M. Wakatsuchi (1998): Formation of 26.8–26.9σ_θ water in the Kuril Basin of the Sea of Okhotsk as a possible origin of North Pacific Intermediate Water. *J. Geophys. Res.*, **103**(C2), 2849–2865.